TEMPERATURE AND FREQUENCY EFFECT ON THE FATIGUE BEHAVIOUR OF SHORT GLASS FIBRE REINFORCED POLYAMIDE 6

A. BERNASCONI, P. DAVOLI – Dipartimento di Meccanica- Politecnico di Milano

A. BASILE, S. GATTI – Radici Novacips – Villa d'Ogna (BG)

ABSTRACT

The effect of temperature and load frequency on the fatigue behaviour of short glass fibre reinforced polyamide 6 has been investigated. Results evidenced the influence of both external and self heating on the fatigue life of specimens, an important aspect for industrial applications.

1. INTRODUCTION

Short glass fibre reinforced polyamide 6 is widely adopted in many industrial applications, e.g. in the automotive industry for under bonnet components like the air intake manifolds, or in electrical and home appliances, where operating temperatures may be higher than room temperature.

The fatigue assessment of mechanical parts requires relations between applied stresses and number of cycles to failure (S-N curves) obtained in a controlled environment and in the correct frequency range.

In fact, due to the visco-elastic behaviour of polymers like the polyamide 6, under cyclic stresses some energy is dissipated, dependent on applied stresses and load frequency, and therefore temperature increases. This self-heating effect is comparable with the effect of external temperature and it has to be taken into account to perform a correct fatigue assessment of mechanical parts [1,2].

The results of fatigue tests on short glass fibre reinforced polyamide 6, that are part of a research programme on the fatigue behaviour of polyamide 6 under different test condition, specimen geometry and fibre orientation [3], are presented and discussed, with particular emphasis on the

cyclic creep fracture surface observations.

2. MATERIALS AND EXPERIMENTAL PROCEDURE

The material investigated is the short glass fibre reinforced (30% weight) polyamide 6. E type glass fibres have a nominal fibre diameter 10 µm and an aspect ratio ranging from 30 to 50. Injection moulding technique was employed for the preparation of specimens.

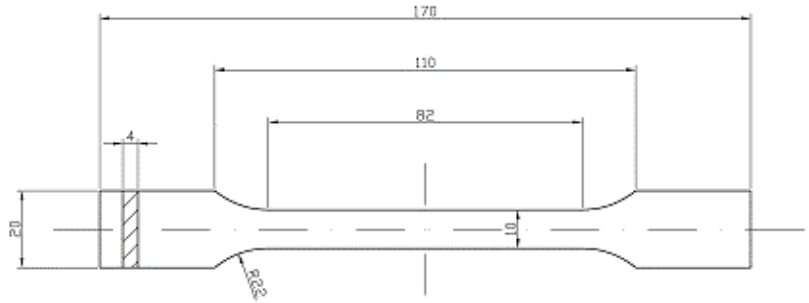

Fig.1: The ISO specimen employed for the tensile and fatigue strength tests

Specimen type and dimensions correspond to the type 1A defined in ISO 527 standard [4] and are reported in Fig. 1.
Specimens were conditioned by submerging them in hot water for four hours and successively keeping them in sealed bags for some weeks, in order to allow for water diffusion. Water content at the end of this accelerated conditioning treatment was 3%.
Tests were carried out employing an MTS 810 servo-hydraulic testing equipment (capacity 100 kN), an environmental chamber for tests at temperatures higher than laboratory room temperature (23°C) and an axial extensometer to record strain values during tests (see Fig.2). To increase the accuracy of load measurements, the test rig was equipped with a 10 kN load cell.

Fig.2: The MTS 810 testing rig, equipped with

environmental chamber and extensometre

Tensile strength and fatigue tests were performed at 23°C and 50°C and the crosshead speed was set at 5 mm/min.
Fatigue tests were conducted in load control mode [5], with sinusoidal tension-tension load cycles at 2Hz and 4Hz. The stress ratio, defined as

$$R = {}^{s_{min}}\!/_{s_{max}} \qquad (1)$$

was kept at a fixed value equal to 0.1.

3. RESULTS AND DISCUSSION

Results of tensile tests at 23°C and 50°C are reported in Tab.1 and in Fig.3: the effect of temperature is a decrease of both ultimate tensile strength and elastic modulus.

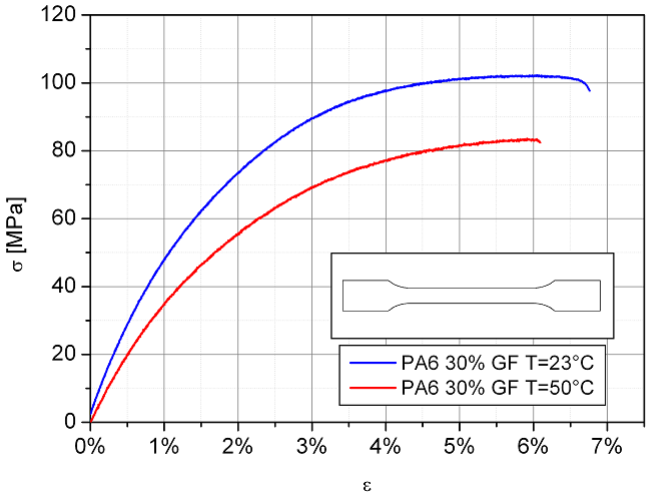

Fig.3: The tensile strength curves of PA6 30% GF at two temperature levels

23°C		50°C	
Rm	E	Rm	E
109 MPa	5800 MPa	84 MPa	4300 MPa

Tab.1: Ultimate tensile stress R_m and elastic modulus E as a function of test temperature

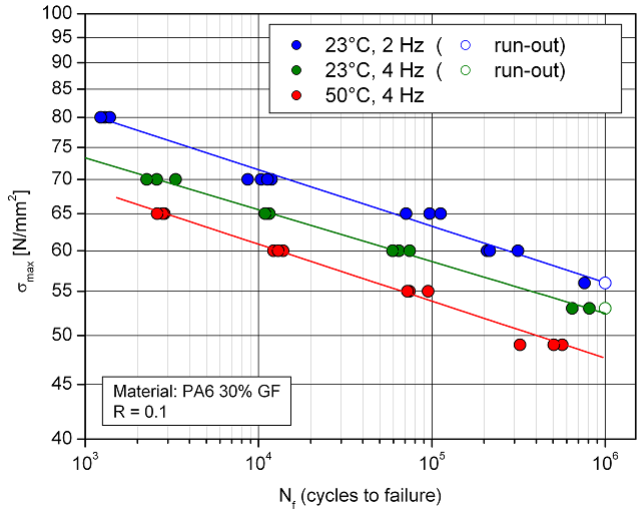

Fig.4: The S-N curves for PA6 30 % GF

The results of fatigue tests are reported in the log-log graph (S-N curves) of Fig. 4, where maximum applied stress values σ_{max} are plotted against the number of cycles to failure N_f. Tests were interrupted after specimen separation or at 10^6 cycles; experimental points corresponding to this last condition are reported as run-outs.
Experimental points are interpolated by a straight line of negative slope k in the log-log graph, thus allowing to extrapolate the fatigue strength at 10^6 cycles values reported in Tab. 2 together with values of the slope k.

The interpolation of data including run-outs required the application of the method of the maximum likelihood.

T@f	s_w	k
23°C@2 Hz	56 MPa	18.9
23°C@4 Hz	52.5 MPa	20.7
50°C@4Hz	47.5	18.5

Tab.2: Fatigue strength at 106 cycles and slope of the S-N curve for the different test conditions

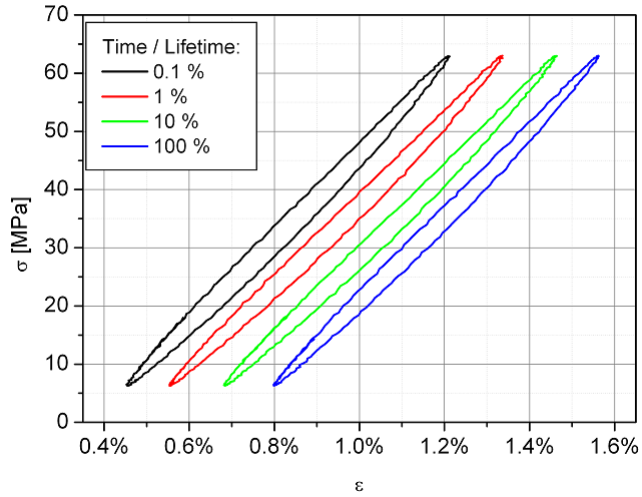

Fig.6: Stress-strain cycles evolution during stress controlled fatigue tests, showing cyclic creep

The effect of increasing test frequency from 2 Hz to 4 Hz is comparable with the reduction of the fatigue strength obtained raising the temperature from 23°C to 50°C at 4 Hz.

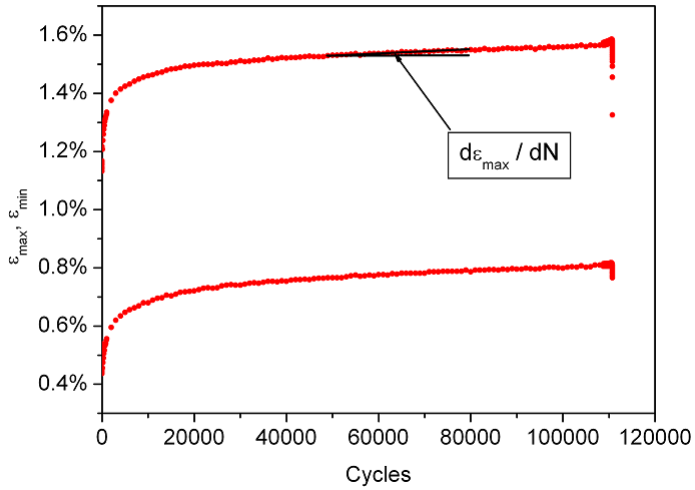

Fig.7: The maximum and minimum strain increase VS time and the definition of the steady state cyclic creep rate of strain accumulation

During each test, strains were measured and recorded. Full stress-strain cycles were stored at fixed intervals, while maximum and minimum strain values were recorded for each cycle.
Due to the visco-elastic behaviour, the phase lag between stresses and strains produces the hysteresis loops of Fig.6. These loops change in position during the experiments (cyclic creep) because of the presence of a mean constant load.
The rate of strain accumulation, i.e. the maximum strain increment per cycle,

$$\dot{\varepsilon} = d\varepsilon_{max} / dN \qquad (2)$$

is constant in the secondary creep region, as shown in Fig. 7. The values calculated for the tested specimen are well correlated with the number of cycles to failure, see Fig. 8.

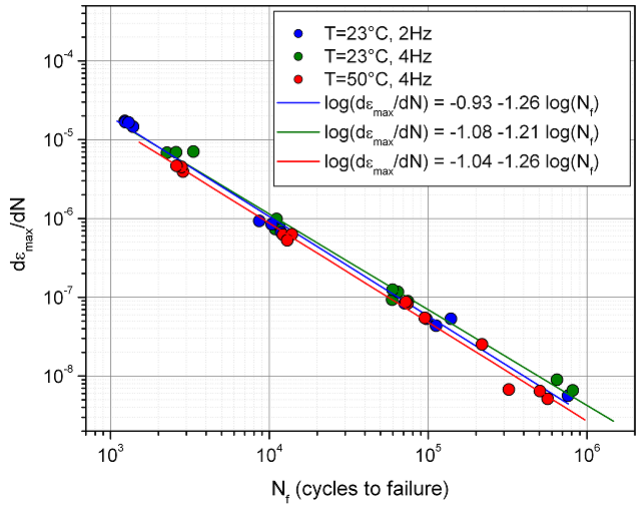

Fig.8: Correlation between cyclic creep maximum strain rate and the number of cycles to failure

The scatter of values is very low, and data from different test condition (temperature and/or frequency) tend to fall on the same line. This correlation may be useful when estimating the residual life for tests interrupted before specimen separation, e.g. for microscope observations.
Fracture surface observations performed employing a scanning electron microscope (SEM) allowed for the identification of the two areas known as micro-ductile and micro brittle [6,7]; they corresponds to the crack nucleation zone and the final fracture surface, respectively.

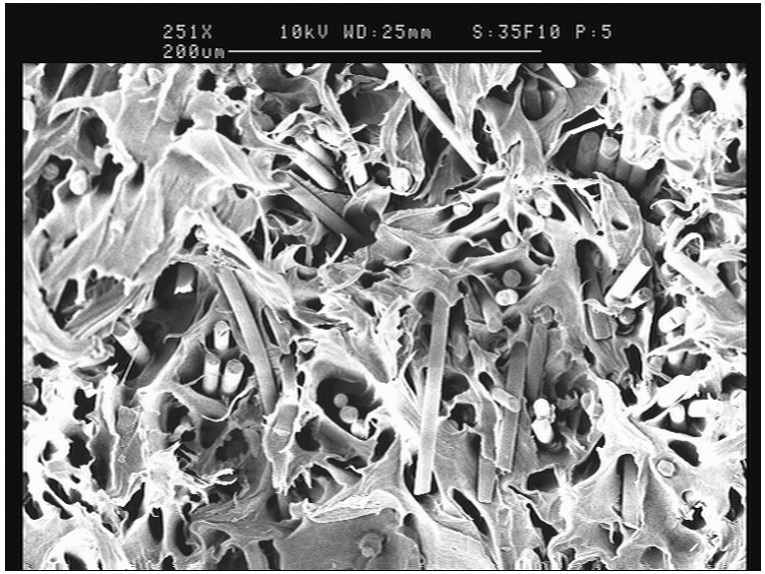

Fig.9: Details of the micro-ductile area of the fracture surface, as observed at SEM

The aspect of the micro-ductile area, see Fig. 9, is characterised by high plastic deformation of the matrix and by fibres pulled out of the matrix, showing no matrix residuals adhering to them, evidence of matrix-fibre interface failure induced by repeated loads.

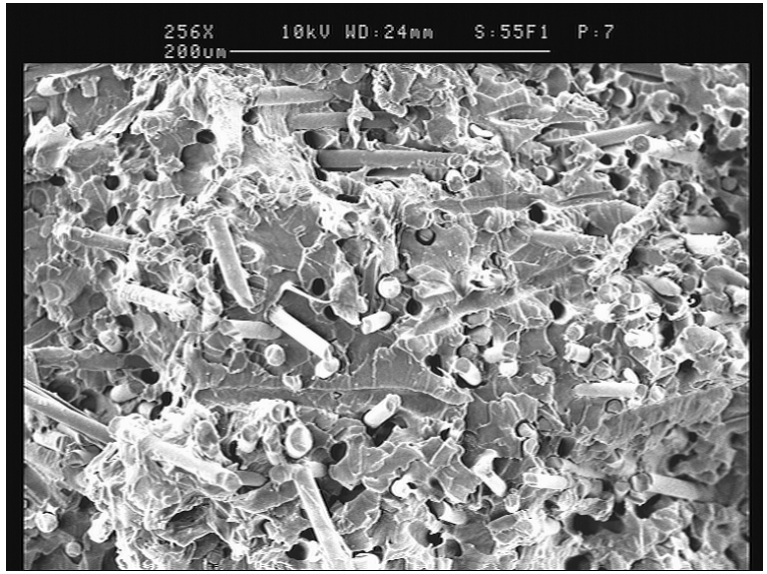

Fig.10: Details of the micro-ductile area of the fracture surface, as observed at SEM

The micro-brittle fracture surface, see Fig. 10, is characterised by small matrix deformation and corresponds to the final fracture of the specimen.
The extension of the micro-ductile area was measured by scanning the fracture surface at high magnification, near the transition between micro-ductile and micro-brittle zones shown in Fig. 11.
The extension of the micro ductile area depends on the type of failure mechanism, which can follow the net section strength criterion, expressed by

$$\sigma_{max} W s = (W - a)\, s R_m \qquad (3)$$

where W indicates the specimen width, s the specimen thickness and a the extension of the micro-ductile area, or the linear elastic fracture mechanics

$$K_I = \sigma_{nom} Y \sqrt{\pi a} = K_{IC} \qquad (4)$$

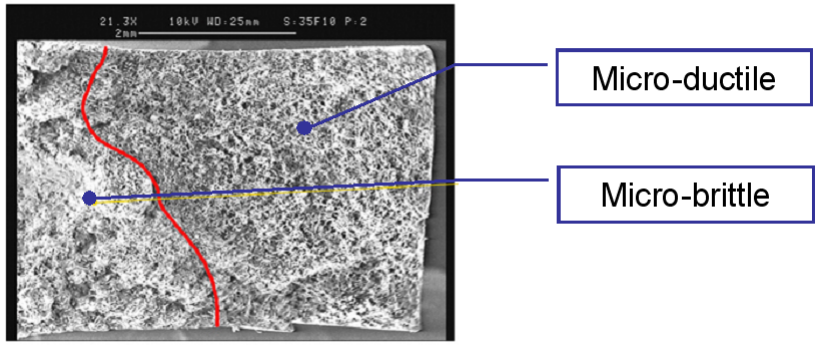

Fig.11: The transition from micro-brittle and micro-ductile zone

When the ductility of the material is high, e.g. when water absorption is induced, as in the case of conditioned specimens, the material follows the net section strength criterion.

This characteristic is visible in Fig. 12, where values of the extension of the micro-ductile area, normalised by dividing them by the specimen width, were reported in a graph against the applied stress, normalised by dividing by the ultimate tensile strength. The points fall on the straight line corresponding to the net section strength criterion.

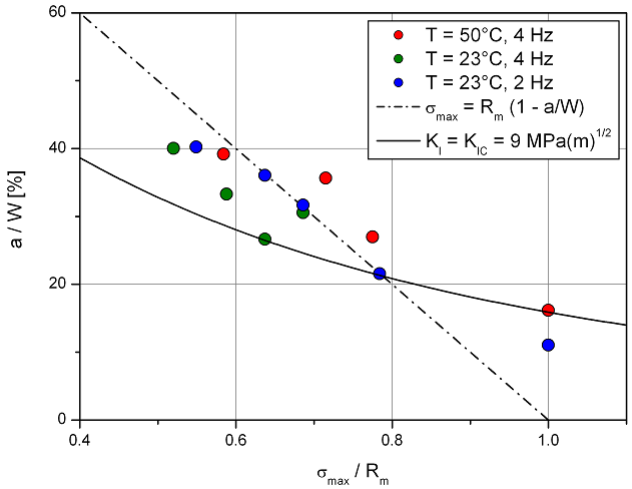

Fig.12: Normalised micro-ductile area values vs normalised applied stress

These results are in good agreement with the behaviour of conditioned specimens described in the literature [6], whereas dry as moulded specimens generally follow the linear elastic fracture mechanics.

4. CONCLUDING REMARKS

The detailed characterisation of the PA6 30% GF in cyclic tension evidenced that lifetimes are strongly dependent on temperature and frequency, but cyclic behaviour and failure mechanism are not modified.

A master S-N curve [8] cannot be derived without considering the visco-elastic behaviour and the temperature increase dependent on the exchange of the heat generated by internal damping that requires the measurement of the temperature the specimen surface with high accuracy.

Future activities of the research programme will involve the study of the effect of notches, fibre orientation, with the aim to develop design tools useful for transferring test results to the design of mechanical parts and components.

BIBLIOGRAPHIC REFERENCES

1. J.F. Mandell. Fatigue behavior of short fiber composite materials, in Fatigue of Composite materials, K.L. Reifsnider editor, Elsevier, 1990
2. K. Handa, A. Kato and I. Narisawa. Fatigue characteristics of Glass-Fiber-Reinforced Polyamide. J

of Applied Polymer Science, Vol. 72, pp. 1783-1793, 1999

3. A.Bernasconi, P. Davoli, A. Basile and S. Gatti Progettare con le poliammidi: la resistenza a fatica della PA6 rinforzata con fibre di vetro. Interplastics, giugno 2003
4. ISO 727-2. Plastics- Determination of tensile properties – Part 2: Test conditions for moulding and extrusion plastics, 1993
5. ASTM D 3479 M-96. Standard Test Method for Tension-Tension Fatigue of Polymer Matrix Composite Materials, 1996
6. J.J. Horst and J.L. Spoormaker. Mechanism of fatigue in short glass fiber reinforced polyamide 6. Polymer engineering and science, Vol. 36, No 22, 1996
7. J.J. Horst and J.L. Spoormaker. Fatigue fracture mechanism and fractography of short-glassfibre-reinforced polyamide 6. J.of Material Science (32), 1997
8. N. Jia and V.A. Kagan. Effects of time and temperature conditions on the tensile-tensile fatigue behavior of short fiber reinforced polyamides. Procs of ANTEC'97, 1997